Journal of Hepatocellular Carcinoma

Dovepress
open access to scientific and medical research

Open Access Full Text Article

ORIGINAL RESEARCH

miR-612 Enhances RSL3-Induced Ferroptosis of Hepatocellular Carcinoma Cells via Mevalonate Pathway

Kailin Xing[1,*], Xinyu Bian[2,*], Dongmin Shi[3,*], Shuangshuang Dong[1], Hongxin Zhou[1], Shuxiu Xiao[4], Jinjin Bai[4], Weizhong Wu[1,4]

[1]Liver Cancer Institute, Zhongshan Hospital, Fudan University, Key Laboratory of Carcinogenesis and Cancer Invasion, Shanghai, 200032, People's Republic of China; [2]Department of Radiation Oncology, Affiliated Hospital of Nanjing University of Chinese Medicine, Nanjing, 210000, People's Republic of China; [3]Department of Medical Oncology, Shanghai Changzheng Hospital, Shanghai, 200072, People's Republic of China; [4]Clinical Center for Biotherapy, Zhongshan Hospital, Fudan University, Shanghai, 200032, People's Republic of China

*These authors contributed equally to this work

Correspondence: Weizhong Wu, Liver Cancer Institute, Zhongshan Hospital, Fudan University, Key Laboratory of Carcinogenesis and Cancer Invasion, Ministry of Education, Shanghai, 200032, People's Republic of China, Tel +86-21-60268628, Fax +86-21-64037181, Email wu.weizhong@zs-hospital.sh.cn

Background: MicroRNA-612 (miR-612) has been proven to suppress the formation of invadopodia and inhibit hepatocellular carcinoma (HCC) metastasis by hydroxyacyl-CoA dehydrogenase alpha subunit (HADHA)-mediated lipid reprogramming. However, its biological roles in HCC cell ferroptosis remain unclear.

Methods and Results: In this study, we found that HCC cells with high metastatic potential were more resistant to ferroptosis, indicating that ferroptosis is related to HCC metastasis. The levels of lipid reactive oxygen species (ROS) were found to be much lower in HCC cells with high metastatic potential by flow cytometry (FCM). We used HCC cells with miR-612 overexpression/knockout and HADHA overexpression/knockdown to test cell viability after stimulation with RSL3. HCC cells overexpressing miR-612 were more sensitive to ferroptosis, and miR-612 could increase lipid ROS levels. Furthermore, colony formation assays and Transwell assays showed that miR-612 could inhibit the proliferation and metastasis of HCC cells by promoting ferroptosis. We next confirmed that miR-612 influenced HCC cell ferroptosis by regulating HADHA. HADHA could upregulate the expression of key enzymes in the mevalonate (MVA) pathway. HADHA overexpression upregulated the expression of CoQ10 and decreased polyunsaturated fatty acid (PUFA) levels and lipid peroxide abundance. miR-612 also suppressed HCC cell proliferation and metastasis by enhancing RSL3- and lovastatin-induced ferroptosis in vivo.

Conclusion: Overall, miR-612 promotes ferroptosis in HCC cells and affects HCC proliferation and metastasis by downregulating CoQ10 and increasing cellular PUFA levels and lipid peroxides via the HADHA-mediated MVA pathway.

Keywords: HCC, Ferroptosis, miR-612, HADHA, MVA pathway

Introduction

Hepatocellular carcinoma (HCC) is one of the most frequent malignant carcinomas.[1,2] Recurrence and metastasis are the key factors influencing the prognosis of HCC patients. Elucidating the mechanism of HCC metastasis and finding new treatment targets are of great importance. Essentially, tumor metastasis is caused by aberrant cell death regulation.[3] Cell death modes, such as apoptosis, necrosis, autophagy, and pyroptosis, can affect cancer metastasis and the prognosis of cancer patients.[4,5]

Ferroptosis is a new kind of cell death discovered in recent years. Distinct from other types of cell death, ferroptosis is characterized by Fe^{2+}-dependent ROS accumulation and lipid peroxidation.[6,7] Specifically, inhibiting the cystine/glutamate transport function of SLC7A11 by erastin, sulfasalazine, and sorafenib or inhibiting glutathione peroxidase 4 (GPX4) by RSL3 could induce an abnormal increase in cellular ROS levels, resulting in the peroxidation of

Received: 1 August 2023
Accepted: 22 November 2023
Published: 6 December 2023

polyunsaturated fatty acids (PUFAs).[8–10] These toxic lipid peroxides, such as lipid peroxyl radical (L-OOH) and lipid alkoxy radical (L-O-), lead to protein and phosphatidylethanolamine (PE) dysfunction in cell membranes.[11,12] In addition, changes in the absorption, transportation, release, and restoration of Fe^{2+} affect the Fenton reaction and activity of Fe^{2+}-containing enzymes and further regulate the process of ferroptosis.[13,14]

However, whether ferroptosis is involved in HCC metastasis and whether targeting ferroptosis can be a new strategy to treat cancer are less known. Recent studies found that tumor cells undergoing epithelial to mesenchymal transition (EMT) were highly sensitive to ferroptosis inducers, suggesting that ferroptosis is involved in tumor metastasis.[15,16] Tumor metastasis is a multistep and low-efficiency process. The dramatic alterations in the oxygen and Fe^{2+} levels of tumor cells during the migration from the primary tumor site to the blood vessels and finally into distant target organs increase their susceptibility to ferroptosis.

MicroRNAs (miRNAs) are endogenous small noncoding RNAs that regulate target gene expression and cell function.[17] Studies suggest that some miRNAs, such as miR-17-92, miR-9, and miR-137, participate in ferroptosis.[18–20] In our previous studies, we found that miR-612 negatively regulated invadopodia formation, EMT, and HCC metastasis by HADHA-mediated lipid reprogramming.[21] By targeting HADHA, miR-612 suppressed the formation of cholesterol via the SREBP2/HMGCR cascade.[22] However, whether the miR-612-HADHA axis affects the ferroptosis of HCC cells is unknown.

In this study, we explored the effect of miR-612 on HCC cell ferroptosis and the underlying mechanism, especially in the process of metastasis, thus providing a new strategy for liver cancer treatment.

Materials and Methods

Reagents

RSL3, ferrostatin-1, Z-VAD-FMK, necrostatin-1, and lovastatin were purchased from MedChemExpress. C11-BODIPY was obtained from Life Invitrogen. Liperfluo and FerroOrange were purchased from Dojindo Molecular Technologies.

Cell Lines and Cell Culture

HCCLM3 cells and MHCC97H cells were maintained at the Liver Cancer Institute, Zhongshan Hospital, Fudan University. Huh7 and HepG2 cell lines were obtained from the Shanghai Cell Bank, Chinese Academy of Sciences. All these cells were cultured in DMEM (Gibco, USA) supplemented with 10% FBS (Gibco, USA) and maintained in a humidified incubator at 5% CO_2 at 37 °C.

Construction of Stable Cell Lines

The miR-612-overexpressing lentivirus (hU6-MCS-Ubiquitin-EGFP-IRES-puromycin) and the corresponding negative control were purchased from GeneChem (Shanghai, China). HCCLM3 cells were infected with miR-612 virus and screened with puromycin (3 μg/mL, Sigma–Aldrich, St. Louis, MO, USA) for two weeks. Huh7-miR-612-KO cells were provided by RujiPhama (Shanghai, China). The endogenous miR-612 knockout sequence was created by CRISPR Biotech Engineering. Briefly, the miR-612 knockout sequence was inserted into the PX459 plasmid vector. The plasmid was transfected into Huh7 cells. After screening with puromycin, the miR-612 knockout cell clone was verified by Western blotting and sequencing.

HADHA-overexpressing lentiviruses (Ubi-MCS-HADHA-3FLAG-SV40-Cherry), HADHA knockdown lentiviruses (hU6-MCS-CMV-shRNA-eGFP), and their corresponding negative controls were purchased from GeneChem (Shanghai, China). HADHA-overexpressing lentiviruses were used to infect Huh7 cells, while knockdown lentiviruses were used to infect HCCLM3 cells. After infection, cells were selected with puromycin (3 μg/mL, Sigma–Aldrich, St. Louis, MO, USA) for two weeks.

Cell Viability Assay

Cell viability was assessed with a Cell Counting Kit-8 (CCK-8; Dojindo, Japan). Cells (3000/well) were seeded in a 96-well plate. After adherence, the cells were treated with RSL3 alone or in combination with different inhibitors (ferrostatin-1 10 μM, Z-VAD-FMK 10 μM, Necstatin-1 1 μM) for 24 h. Each well was replaced with 100 μL of fresh

DMEM plus 10 μL of CCK-8. Following incubation for 2 h at 37 °C, the optical density value was determined using a microplate reader (Thermo Fisher Scientific, USA) at 450 nm.

Colony Formation Assay

Cells (1000 cells/plate) were seeded in 6-well plates and grown for 2 weeks before being fixed with 4% paraformaldehyde for 15 min at room temperature. The cells were washed three times with PBS and stained with crystal violet (Sigma–Aldrich, USA). Cell colony images were captured, and the colony numbers were counted.

Transwell Migration and Invasion Assay

Cell migration and invasion were examined using Transwell migration and Matrigel invasion assays. Transwell chambers (Corning, USA) were placed in 24-well culture plates. Two hundred microliters of FBS-free DMEM with 1×10^4 cells was added to the upper Transwell chamber, and 600 μL of DMEM with 10% FBS was added to the lower chamber. RSL3 (0.5 μM/L) or DMSO was also added to the upper chamber. After culturing for 48 h, the cells that passed through the Transwell insert were fixed with 4% paraformaldehyde, stained with crystalline medium and then observed by microscopy.

RNA Isolation and qRT–PCR

Total RNA was extracted from cell lines with an RNA purification kit (EZBioscience, USA). Then, 1 μg of total RNA was used for first-strand DNA synthesis with a PrimeScript™ RT reagent kit (Takara, Japan). Real-time PCR was performed employing a Hieff™ qPCR SYBR Green Master Mix kit (Yeasen, Shanghai, China) according to the manufacturer's instructions. GAPDH was used as an internal control. The primers for the genes of interest were synthesized by Sangon Biotech, as shown in Table 1.

Western Blot Analysis

For Western blot assays, whole cell lysates were prepared in modified lysis buffer (50 mM Tris·HCl, pH 6.8, 2% SDS) supplemented with phosphatase and protease inhibitors (Roche, Mannheim, Germany). Equal amounts of total proteins were subjected to 10% SDS polyacrylamide gels and transferred to polyvinylidene difluoride membranes. The membranes were incubated with primary antibodies at 4 °C overnight and horseradish peroxidase–conjugated secondary antibodies at room temperature for 1 hour. Enhanced chemiluminescence assays were applied to detect the signal. Antibodies that bind to HADHA (11,052-1-AP), SREBP2 (11,224-1-AP), HMGCS1 (14,295-1-AP), HMGCR (11,064-1-AP), MVD (11,880-1-AP), MVK (11,263-1-AP), FPPS (15,073-1-AP), and GGPS1 (26,158-1-AP) were purchased from Proteintech (Wuhan, China). Goat anti-rabbit or anti-mouse secondary antibodies were obtained from Beyotime Biotechnology (Shanghai, China).

Flow Cytometric Analysis

Cells were seeded in 6-well plates and treated with RSL3 (1 μM) for 6 h. Cells were collected and washed with Hanks balanced salt solution (HBSS, Gibco). Cells were then resuspended in 400 μL of HBSS containing 2 μM C11-BODIPY

Table 1 PCR Primer Sequences

Gene	Sequence
Hsa-miR-612	5'- GCAGGGCTTCTGAGCTCCTTAA −3'
U6 small nuclear RNA (U6)	5'- CAAATTCGTGAAGCGTTCCATAT −3
HADHA	
Forward	5'-AGTAGAAGCGGTGATTCCAGA-3'
Reverse	5'-CCACGGGAGAGAAGTAGTGC-3'
GAPDH	
Forward	5'-CACCATGAAGATCAAGATCATTGC-3'
Reverse	5'-GGCCGGACTCATCGTACTCCTGC-3'

and incubated for 10 min at 37 °C in a culture incubator. Subsequently, the supernatant was removed, and the cells were resuspended in 500 μL of PBS. Finally, the lipid-ROS level was analyzed with a flow cytometer (Beckman Coulter).

Lipid ROS and Fe^{2+} Detection by High-Content Screening Microscopy

Cells were seeded in 96-well plates and treated with RSL3 (1 μM) or DMSO for 6 h. For lipid ROS detection, Liperfluo (1 mM) was added to the culture, incubated for 30 min at 37 °C and then analyzed by high-content screening microscopy. For Fe^{2+} detection, cells were washed with HBSS 3 times and incubated in FerroOrange (1 μM) for 30 min at 37 °C. Then, the cells were analyzed by high-content screening microscopy.

Xenograft Mouse Model

Five-week-old nude mice (BALB/c) were purchased from Shanghai Laboratory Animal Co. Ltd. (China) and randomly divided into two groups (n = 12/group): (1) the NC group and (2) the HCCLM3 miR-612OE group. Cells (6×10^6) were subcutaneously injected into the nude mice. When the tumor sizes reached approximately >50 mm^3, the mice in each group were further randomly divided into 4 subgroups (n=3/group): (A) DMSO group; (B) lovastatin group; (C) RSL3 group; and (D) lovastatin+RSL3 group. Group B was intraperitoneally injected with 50 mg/kg lovastatin every Tuesday and Friday for 3 weeks. Group C was intratumorally injected with 100 mg/kg RSL3 every Thursday and Sunday for 3 weeks. Group D was treated with both Group B and Group C regimens. Mice in Group A were treated with an equal volume of DMSO. Simultaneously, tumor formation was monitored, and the tumor size was calculated using the formula $V = 0.5 \times L \times W^2$ (L, length and W, width). At the end of this experiment, the mice were euthanized, and their tumor tissues were isolated. The animal experiments were carried out in accordance with the Guidelines for the Care and Use of Laboratory Animals and approved by the Institutional Review Board of Zhongshan Hospital of Fudan University.

Mass Spectrometry Assay

Cells were seeded in 10 cm culture dishes and treated with RSL3 (1 μM) for 6 h. Cells were collected and washed with PBS. Every sample collected 3 dishes of cells and counted to be 1×10^8. Sample placed in liquid nitrogen for 2 min, then thawed on ice for 5 min and vortex blending. Repeated 3 times, then centrifuged with 5,000 rpm at 4°C for 1 min. Homogenized with 1mL mixture (include methanol, MTBE and internal standard mixture). Whirled the mixture for 15 min. Then added 200 μL of water and whirled the mixture for 1 min, and centrifuged with 12000 rpm at 4°C for 10 min. Extracted 500 μL supernatant and concentrated it. Dissolved powder with 200 μL mobile phase B, then stored in −80°C. Finally took the dissolving solution into the sample bottle for LC-MS/MS analysis.

For the analysis of oxidized lipids, cells were spiked with 200 μL of oxidized lipid extract, vortexed for 5 minutes and the protein was precipitated at low temperature (−20°C). Then spiked with 20 μL of 1 μM internal standard mixture to each sample and vortexed for 10 min, centrifuged at 5000 rpm for 10 min at 4 °C, repeated the extraction once and combined the supernatants. The eicosanoids in supernatants were extracted using Poly-Sery MAX SPEcolumns (ANPEL). Prior to analysis, the eluent was dried under vacuum and redissolved in 100μL of methanol/water (1:1, v/v) for UPLC/MS/MS analysis.

Statistical Analysis

Data were analyzed using SPSS 24.0 and GraphPad 8.0. Quantitative variables were expressed as the mean ± SD. Student's *t* test was used to compare differences between two groups. Comparisons among multiple groups were performed by one-way ANOVA. $p < 0.05$ was considered statistically significant.

Results

RSL3 Induces Ferroptosis in HCC Cells

HCC cells with different metastatic potentials were treated with RSL3 at different concentrations (0, 0.1, 0.5, 1, 2 μM) for 24 h. Cell viability was examined by CCK-8 assay. The results showed that RSL3 significantly reduced the viability of HCC cells in a dose-dependent manner (Figure 1A). This process could be reversed by a ferroptosis inhibitor

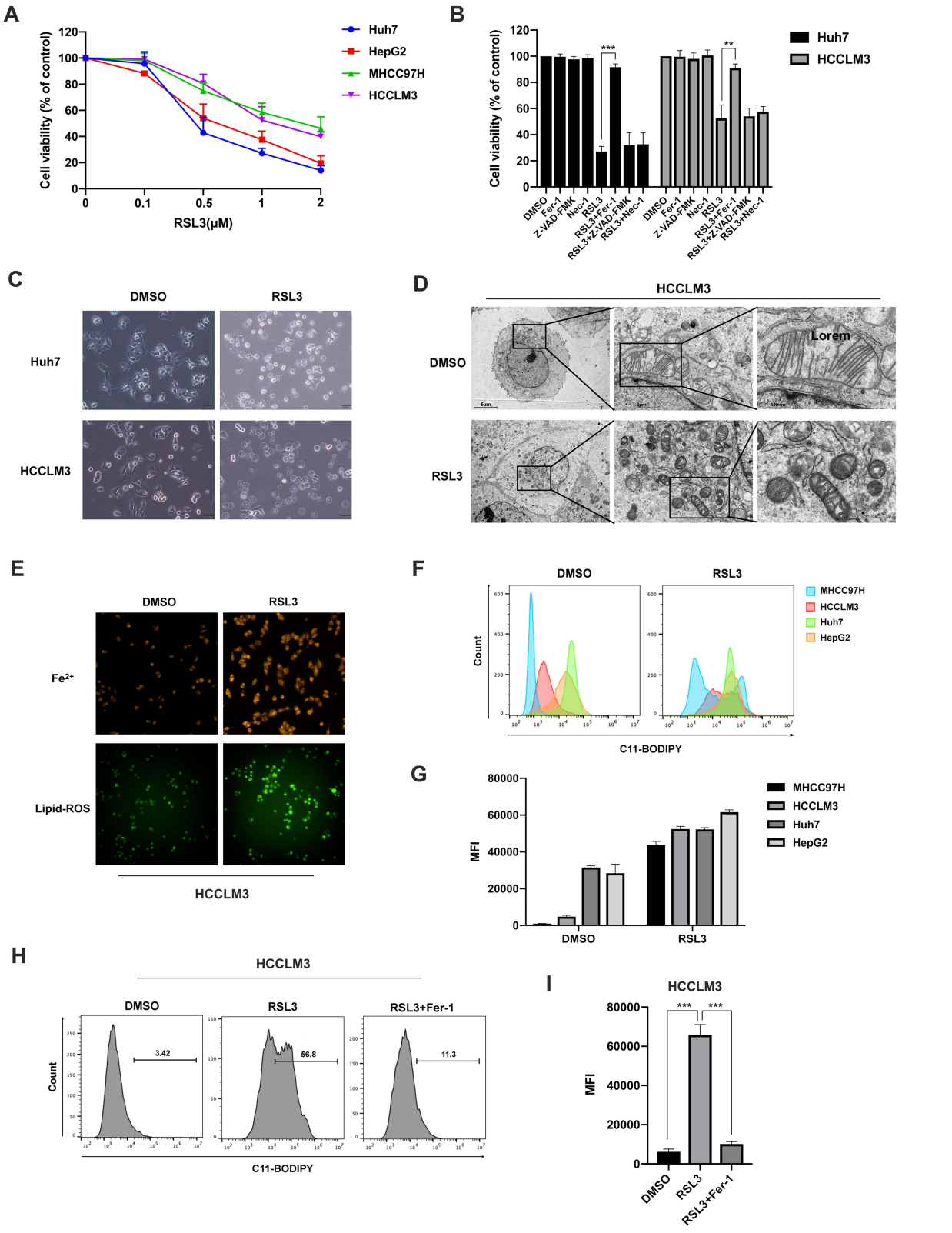

Figure 1 RSL3 induced ferroptosis in HCC cells. (**A**) RSL3 induced HCC cell death in a dose-dependent manner, and cells with lower metastatic potentials (Huh7, HepG2) were more sensitive to RSL3. (**B**) Cell death induced by RSL3 could be reversed by Fer-1 but could not be reversed by ZVAD-FMK and necrostatin-1. ** p<0.01, *** p<0.001. (**C**) Images of HCC cells treated with RSL3 (1 μM) and DMSO (contrast) for 24 h observed by optical microscopy. (**D**) Transmission electron microscopy of HCCLM3 cells treated with RSL3 (1 μM, 6 h). (**E**) Representative images of HCCLM3 cells treated with 1 μM RSL3 for 6 h. Cells were fixed and stained after 6 h of RSL3 treatment. The images were captured using high-content screening microscopy. Orange, FerroOrange. Green, Liperfluo. Scale bar, 100 μm. (**F**). (**G**). Lipid ROS levels were analyzed by FCM in HCC cells with different metastatic potentials. (**H**). (**I**). Lipid ROS levels were analyzed by FCM in HCCLM3 cells treated with RSL3 (1 μM) ±Fer-1 (10 μM). ***p<0.001.

(ferrostatin-1 (Fer-1), 10 μM) but not an apoptosis inhibitor (ZVAD-FMK, 10 μM) or a necroptosis inhibitor (necrostatin-1, 1 μM) (Figure 1B), showing that RSL3 could induce ferroptosis in HCC cells. Furthermore, we found that cells with lower metastatic potential (Huh7 and HepG2) were more sensitive to ferroptosis than cells with higher metastatic potential (HCCLM3 and MHCC97H), indicating that ferroptosis was related to HCC metastasis (Figure 1A). We next observed morphological changes in HCC cells induced by RSL3. Most of the cells treated with RSL3 (1 μM) for 24 h were dead and detached from the plate by optical microscopy, while the control cells grew well (Figure 1C). Using transmission electron microscopy, we observed the intracellular structure in RSL3-treated (1 μM, 6 h) HCCLM3 cells. Compared to the DMSO-treated group, the RSL3-treated cells had smaller mitochondria with increased density, but the cell membrane remained intact (Figure 1D).

Ferroptosis is characterized by the iron-dependent accumulation of ROS. Therefore, we investigated changes in iron and lipid ROS levels in HCCLM3 cells. Following RSL3 treatment, both iron and lipid ROS levels were increased, as observed by high-content screening microscopy (Figure 1E). We further analyzed lipid ROS levels by FCM. After RSL3 induction, lipid ROS levels were increased in HCC cells. And cells with higher metastatic potential (HCCLM3, MHCC97H) had much lower lipid ROS levels than cells with lower metastatic potential (Huh7, HepG2) (Figure 1F and G). The results also showed that RSL3-induced lipid ROS accumulation could be abrogated by Fer-1 in HCCLM3 cells (Figure 1H and I).

miR-612 Enhances RSL3-Induced Ferroptosis in HCC Cells

In our previous study, we found that miR-612 was expressed at low levels in HCCLM3 cells and endogenously expressed at high levels in Huh7 cells.[21] To explore the effect of miR-612 on HCC ferroptosis, we overexpressed miR-612 in HCCLM3 cells and knocked out miR-612 in Huh7 cells. Real-time PCR showed that miR-612 was significantly upregulated in HCCLM3$^{miR-612-OE}$ cells and downregulated in Huh7$^{miR-612-KO}$ cells (Figure 2A). Next, we treated miR-612 OE and KO cells with RSL3 and examined their viability with a CCK-8 assay. The results showed that the

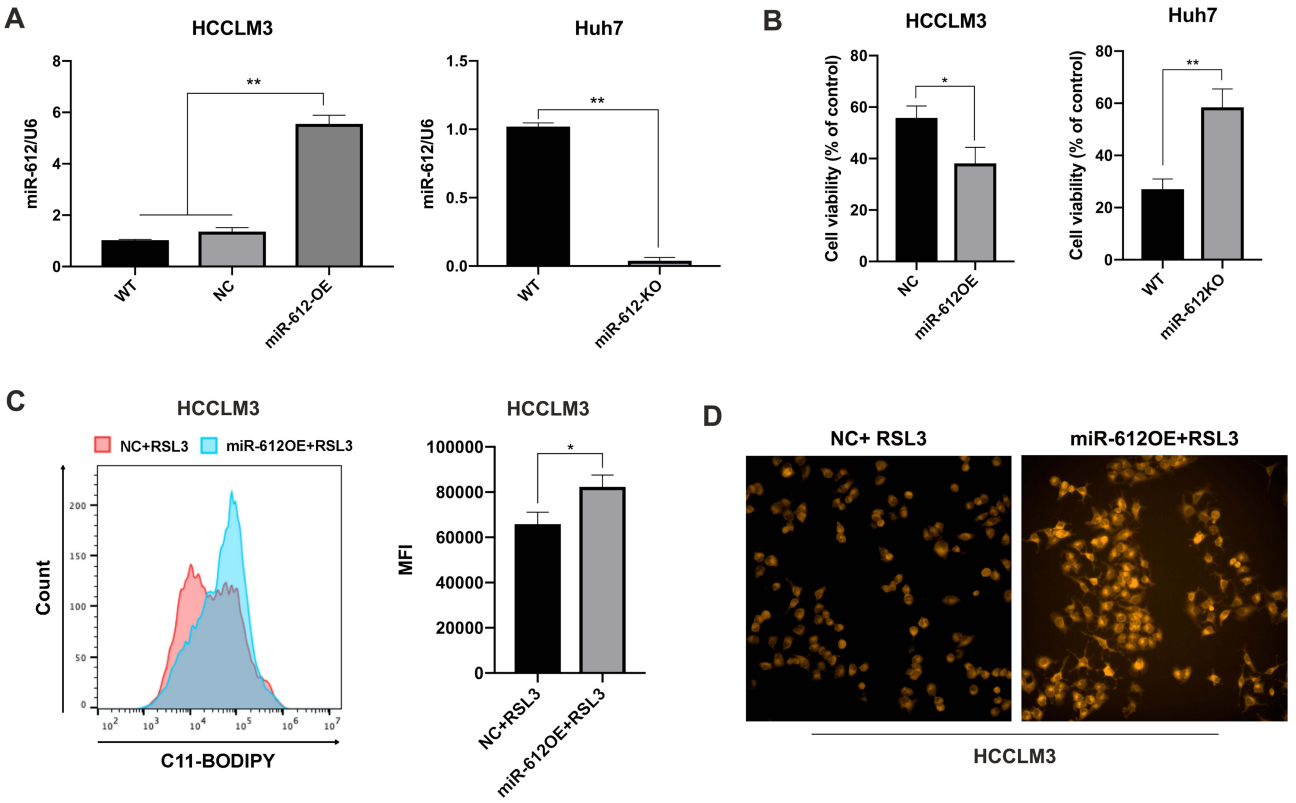

Figure 2 miR-612 enhances RSL3-induced ferroptosis in HCC cells. (**A**) Real-time PCR analysis of miR-612 expression in HCCLM3$^{miR-612-OE}$ and Huh7$^{miR-612-KO}$ cells. ** p<0.01. (**B**) The effects of miR-612 on HCC ferroptosis induced by RSL3 (1 μM, 24 h) analyzed by CCK8. * p<0.05, ** p<0.01. (**C**) Lipid ROS levels were increased in miR-612-OE cells, as analyzed by FCM. * p<0.05. (**D**) Fe^{2+} accumulation was observed by high-content screening microscopy.

viability of miR-612-OE cells was significantly decreased in the HCCLM3 cell group compared with the control group. In the Huh7 cell group, the viability of miR-612 KO cells was increased compared with that of the control group, indicating that miR-612 enhanced RSL3-induced ferroptosis in HCC cells (Figure 2B). FCM analysis showed that RSL3 increased lipid ROS levels in miR-612-OE cells compared to those in control cells (Figure 2C). Fe^{2+} accumulation was also observed by high-content screening microscopy (Figure 2D).

miR-612 Suppresses HCC Proliferation, Migration and Invasion by Promoting Ferroptosis

The proliferation ability of cells is an important factor in promoting tumor metastasis. We performed a colony formation assay and found that the number of cell colonies was significantly decreased in RSL3-treated HCCLM3 cells compared with control HCCLM3 cells, (Figure 3A, 459.3±44.6 vs 197±36.76, $p<0.01$) and similar results were found in Huh7 cells (Figure 3A, 424.3 ±26.01 vs 101.0±29.51, $p<0.01$). In miR-612-OE cells, cell colony numbers were further reduced (197±36.76 vs 71.33±18.23, $p<0.01$), while they were increased in miR-612-KO cells treated with RSL3 (101.0±29.51 vs 239.3±33.01, $p<0.01$) (Figure 3A). These results illustrated that miR-612 suppresses HCC cell proliferation by promoting RSL3-induced ferroptosis. We also performed Transwell assays to investigate whether miR-612-enhanced ferroptosis could influence HCC cell migration and invasion. The number of $Huh7^{miR-612-KO}$ cells in the migration and invasion assays was approximately 3- or 2.6-fold greater than that of the corresponding control cells (Figure 3B). In the $HCCLM3^{miR-612-OE}$ group, the numbers of successfully migrated and invaded cells were approximately 0.3-fold higher than that of the corresponding control cells (Figure 3B). These results indicated that miR-612 could suppress HCC cell migration and invasion by promoting RSL3-induced ferroptosis.

miR-612 Regulates HCC Ferroptosis via HADHA

In our previous study, we found that miR-612 directly targets HADHA.[22] miR-612 could suppress the mevalonate (MVA) pathway by inhibiting HADHA, thus reducing the formation of cholesterol. CoQ10 acts as a key factor in ferroptosis by deoxidizing free radicals and inhibiting oxidation. Ferroptosis suppressor protein 1 (FSP1) plays an important role in suppressing ferroptosis. CoQ10 is mainly produced by the MVA pathway. Therefore, we hypothesized that miR-612 may suppress the formation of CoQ10, thus promoting ferroptosis.

We have previously proven that HADHA was endogenously expressed at high levels in HCCLM3 cells and at low levels in Huh7 cells.[22] To explore the effect of HADHA on HCC ferroptosis, we generated $HCCLM^{HADHA-KD}$ and $Huh7^{HADHA-OE}$ stable cell lines. Real-time PCR and Western blot assays showed that HADHA was significantly upregulated and down-regulated in $HCCLM^{HADHA-KD}$ and $Huh7^{HADHA-OE}$ cells (Figure 4A and B). Then, we treated HADHA-OE cells, HADHA-KD cells and their control cells with RSL3 and examined their viability. The results showed that the viability of HADHA-OE cells was significantly increased compared with that of control cells and that the viability of HADHA-KD cells was significantly decreased compared with that of control cells (Figure 4C). FCM analysis showed that RSL3 decreased lipid ROS levels in HADHA-OE cells and increased lipid ROS levels in HADHA-KD cells compared to those in control cells (Figure 4D). To further confirm the effects of HADHA on miR-612-mediated ferroptosis, we generated HADHA synonymous mutant cells. HADHA levels were largely rescued in $HCCLM3^{miR-612-OE}$ cells after cotransfection with mutant *hadha*. In contrast, HADHA levels were inhibited by *hadha*-shRNA in $Huh7^{miR-612-KO}$ cells. Indeed, ferroptosis resistance of $Huh7^{miR-612-KO}$ cells was partially compromised after cotransfection with *hadha*-shRNA (Figure 4E). Similarly, enhanced sensitivity to ferroptosis in $HCCLM3^{miR-612-OE}$ cells was partially compromised when cotransfected with a synonymous mutant of *hadha* (Figure 4E). Lipid ROS levels by FCM analysis showed consistent results and indicated ferroptosis after RSL3 induction (Figure 4F). All these findings demonstrated that miR-612 promotes cell ferroptosis mediated by HADHA.

HADHA Increased the Levels of CoQ10 via the MVA Pathway

3-Hydroxy-3-methylglutaryl-coenzyme A synthase 1 (HMGCS1), hydroxymethylglutaryl coenzyme A reductase (HMGCR), mevalonate diphosphate decarboxylase (MVD), mevalonate kinase (MVK), farnesyl diphosphate synthase (FPPS), geranylgeranyl diphosphate synthase 1 (GGPS1) and regulatory factor sterol regulatory element-binding protein 2 (SREBP2) are key enzymes in the MVA pathway. We examined the effect of miR-612 and HADHA on MVA pathway-

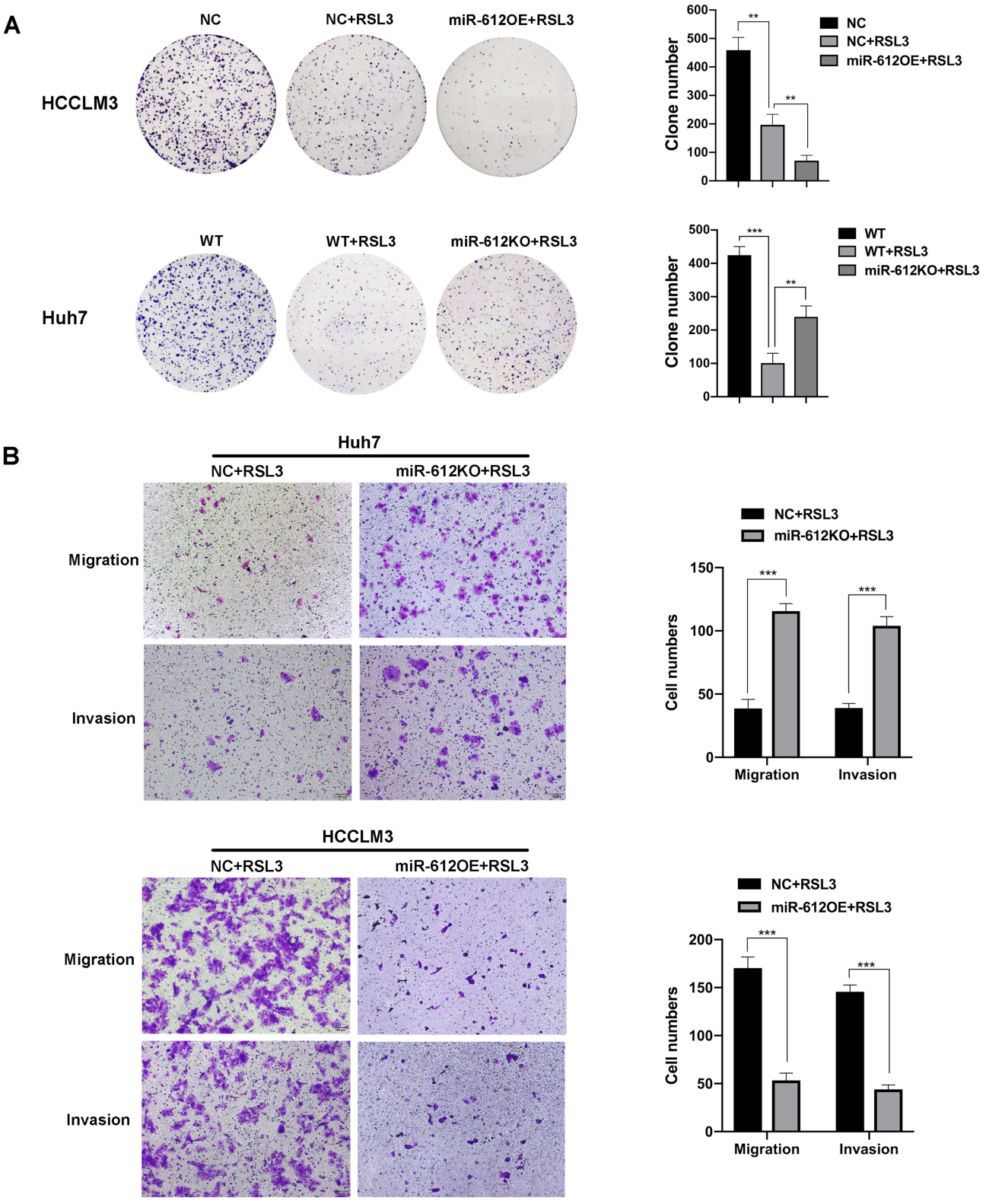

Figure 3 Effects of enhanced ferroptosis by miR-612 on HCC proliferation, migration and invasion. (**A**) Colony formation abilities and statistical results of RSL3-treated Huh7$^{miR-612-KO}$ and HCCLM3$^{miR-612-OE}$ cells. ** p<0.01, *** p<0.001. (**B**) Cell migration and invasion abilities and statistical results of Huh7$^{miR-612-KO}$ and HCCLM3$^{miR-612-OE}$ cells. Scale bars, 200 μm. *** p<0.001.

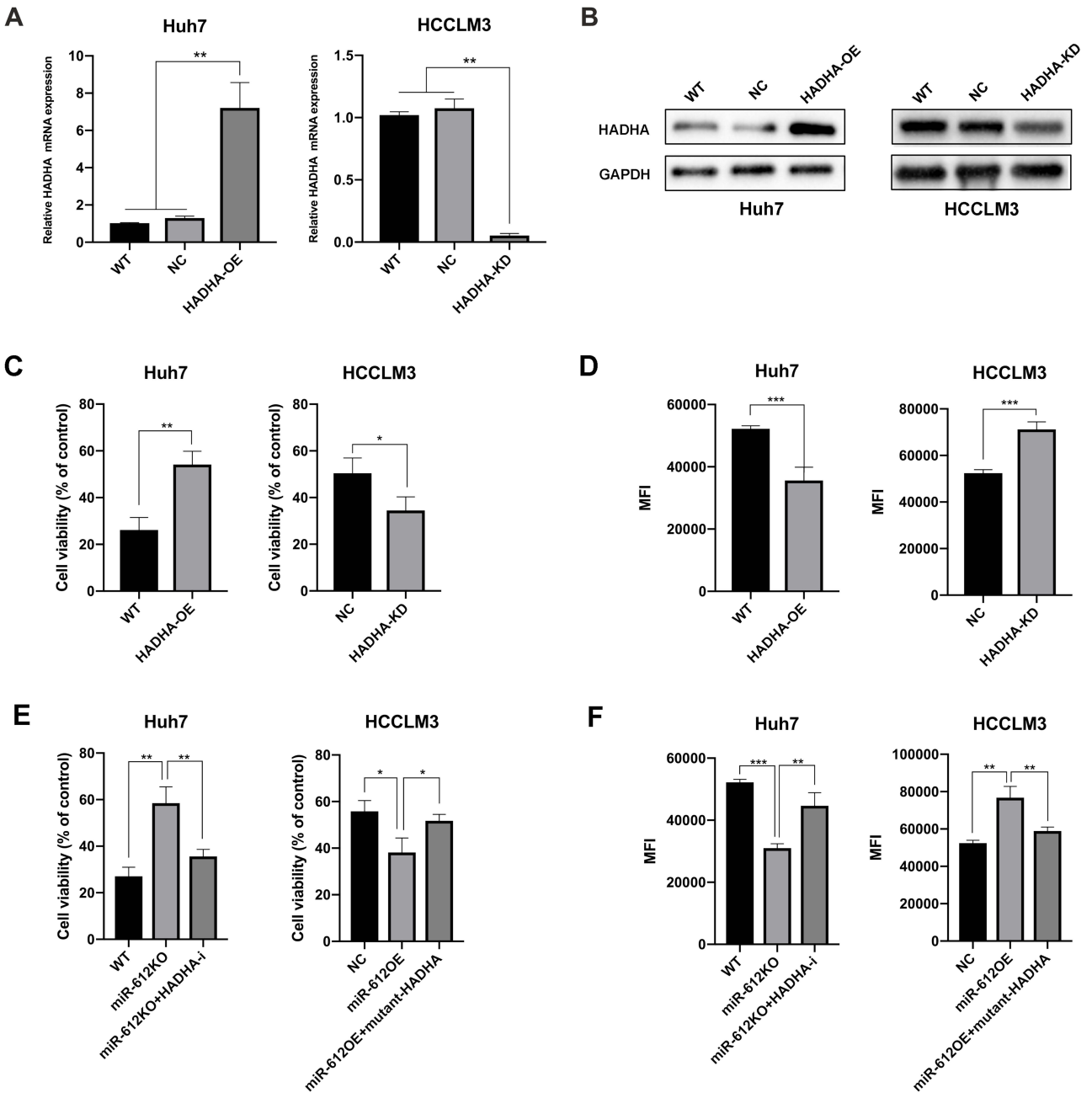

Figure 4 miR-612 regulates HCC ferroptosis via HADHA. (**A**), (**B**) Real-time PCR and Western blot analysis of HADHA mRNA and protein expression in HCCLM$^{HADHA-KD}$ and Huh7$^{HADHA-OE}$ cells. ** p<0.01. (**C**) The effects of HADHA on HCC ferroptosis induced by RSL3 (1 μM, 24 h) were analyzed by CCK-8 assay. * p<0.05, **p<0.01. (**D**) Lipid ROS levels were decreased in HADHA-OE cells and increased in HADHA-KD cells, as analyzed by FCM. *** p<0.001. (**E**) CCK-8 analysis of miR-612 on HCC ferroptosis induced by RSL3 (1 μM, 24 h) after HADHA rescue. * p<0.05, ** p<0.01. (**F**) FCM analysis of lipid ROS in miR-612 OE/KO cells after HADHA rescue. **p<0.01. *** p<0.001.

related proteins by Western blotting. The results showed that the expression of MVA pathway-related proteins was significantly upregulated after miR-612 knockout or HADHA overexpression in Huh7 cells. These proteins were downregulated in miR-612-OE or HADHA-KD HCCLM3 cells (Figure 5A). These results showed that HADHA could promote MVA pathway activation. We further explored whether HADHA could regulate CoQ10, which is the downstream metabolite of the MVA pathway. By mass spectrometry, we found that HADHA could affect the formation of CoQ10. In Huh7$^{HADHA-OE}$ cells, CoQ10 levels were significantly increased compared with those in control cells, while CoQ10 levels in HCCLM3$^{HADHA-KD}$ cells were significantly decreased compared with those in control cells (Figure 5B).

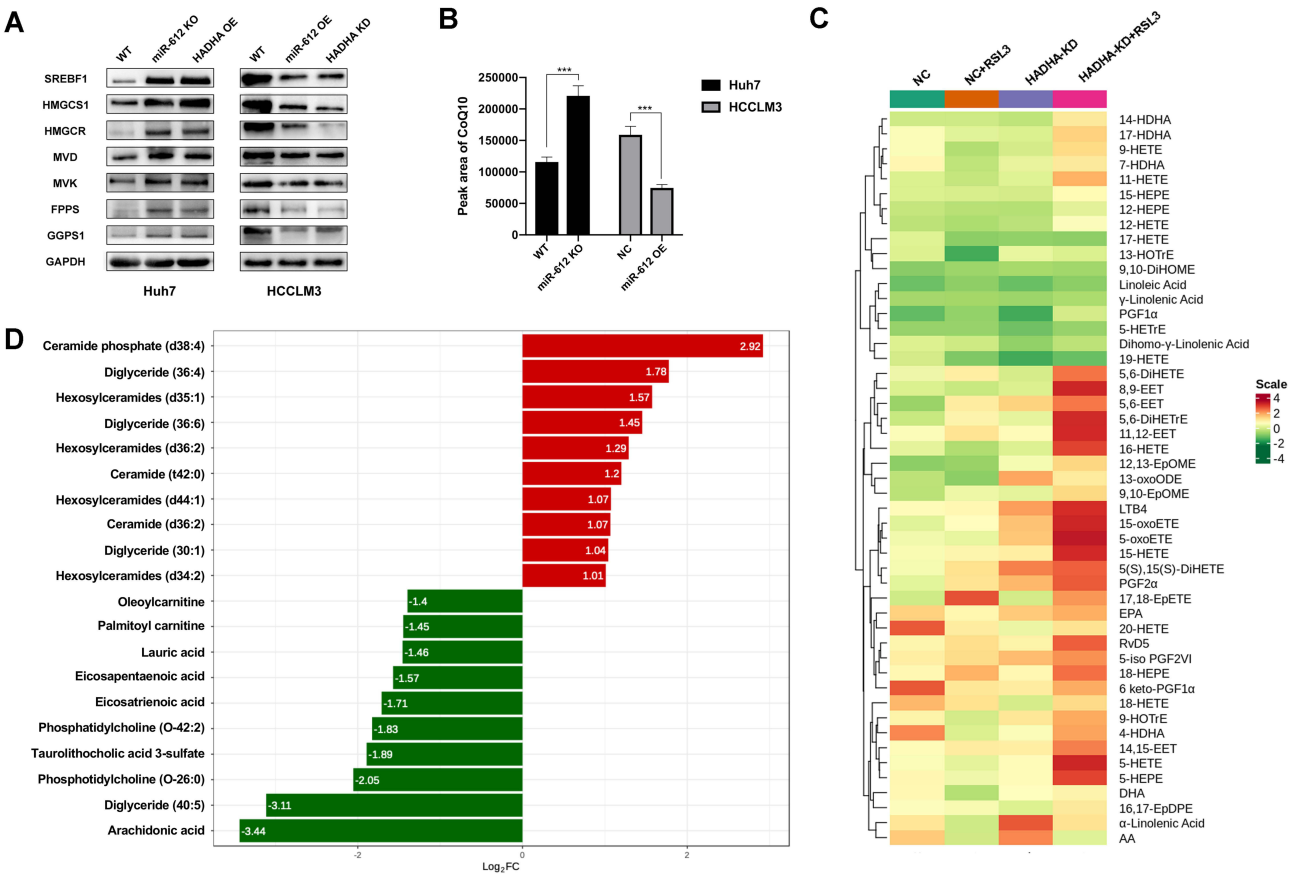

Figure 5 Effects of HADHA on the MVA pathway and HCC cell lipid metabolism. (**A**) Western blot analysis of the effects of HADHA on key enzymes in the MVA pathway. (**B**) HADHA upregulates CoQ10, as analyzed by mass spectrometry. *** p<0.001. (**C**) Heatmap showing that HADHA decreases the abundance of oxidized lipids after RSL3 induction. (**D**) Changes in lipid metabolites in HADHA-overexpressing cells.

HADHA Influences HCC Lipid Metabolism

It has been reported that lipid peroxides, especially hydrogen peroxide, can mediate ferroptosis by destroying the lipid bilayer of the cellular membrane. Lipidomics has shown that phosphatidylethanolamines (PEs) and docosatetraenoic acid (DHA) containing arachidonic acid (AA) are critical lipids that drive ferroptosis. Moreover, oxidative lipid metabolism plays an important role in ferroptosis. Therefore, we further explored the impact of HADHA on HCC cell oxidative lipid metabolism.

We first tested Huh7$^{\text{HADHA-OE}}$ cells and control cells using the widely targeted quantitative lipidomics method by mass spectrometry. The results showed that the levels of lipids such as ceramide and diglyceride were significantly increased in HADHA-overexpressing cells, whereas the levels of PUFAs such as DHA, epoxyeicosatrienoic acid (EPA), and AA were significantly decreased (Figure 5D). These results clarified that HADHA could promote the formation of saturated lipids and reduce the level of PUFAs, thus inhibiting ferroptosis.

Next, we quantitively examined 71 oxidized lipids, including downstream oxidized metabolites originating from AA, linoleic acid (LA), α-linolenic acid (ALA), DHA, EPA and dihomo-gamma-linolenic acid (DGLA), in HCCLM3 cells before and after RSL3 induction. The results showed that the abundance of oxidized lipids in HCC cells was significantly enhanced after RSL3 induction, and this phenomenon was much more obvious in HADHA-KD cells (Figure 5C). Conclusively, HADHA could effectively inhibit ferroptosis by reducing the abundance of oxidized lipids.

miR-612 Augments the Tumor Inhibitory Effect of RSL3 and Lovastatin in vivo

Our previous study demonstrated that RSL3-induced ferroptosis could inhibit HCC cells and that miR-612 could promote ferroptosis by suppressing the MVA pathway. We further constructed a subcutaneous xenograft model in nude mice to verify these data in vivo. Lovastatin is an effective HMG-CoA reductase inhibitor that inhibits the MVA pathway.

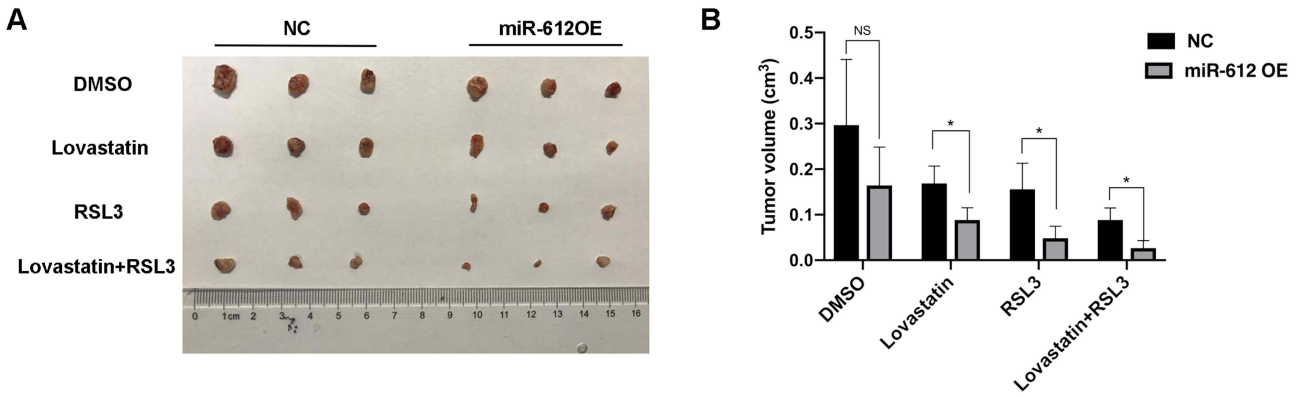

Figure 6 Effects of miR-612 on RSL3 and lovastatin in vivo. Macrograph (**A**) and absolute volume (**B**) of subcutaneous xenograft tumors in different groups. * p<0.05.
Abbreviation: NS, not significant.

Control and miR-612-overexpressing HCCLM3 cells were subcutaneously injected into nude mice. We found that in both the control and miR-612OE groups, RSL3 and lovastatin markedly suppressed the growth of tumors (Figure 6), indicating that RSL3 and lovastatin effectively and synergistically inhibited tumors. We also found that compared with tumor growth in the control group, tumor growth in the miR-612OE group were further suppressed (Figure 6), suggesting that miR-612 could enhance ferroptosis induced by RSL3 and lovastatin and augment the tumor inhibitory effect of RSL3 and lovastatin in vivo.

Discussion

Tumor metastasis is a complicated process and is still the main obstacle to treating cancers. Recent studies have provided new insights into the relationship between ferroptosis and tumor metastasis.[23–25] Inducing ferroptosis in tumor cells could be a potential way to inhibit tumor metastasis and thus treat cancer. Our study explored the of miR-612 on HCC cell ferroptosis and HCC metastasis, which provides evidence for a new strategy for HCC treatment.

In our study, we found that HCC cells with high metastatic potential were more resistant to ferroptosis. By analyzing lipid ROS levels, we found that the level of lipid ROS was much lower in HCC cells with high metastatic potential, showing that these cells possessed a more potent antioxidant system and were more resistant to ROS. It is well known that ROS play important roles under both physiological and pathological conditions and directly initiate ferroptosis. Recent studies suggest that tumor cells resistant to ROS can be more susceptible to the metastasis,[26] which was in line with our study. These results encourage us to find new ways to regulate ROS and ferroptosis to suppress HCC metastasis.

It has been established that miR-612 could regulate HCC metastasis by HADHA-mediated lipid reprogramming.[22] HADHA promotes β-oxidation of fatty acids and cholesterol synthesis in HCC. CoQ10, also named ubiquinone, traps oxygen radicals and prevents the oxidation of proteins, lipids and DNAs by transferring hydrogen to free radicals.[27–29] CoQ10 acts as a crucial antioxidant factor as well as ferroptosis inhibitor by reducing the abundance of cellular lipid peroxides.[30–32] Considering that both cholesterol and CoQ10 are mainly biosynthesized by the MVA pathway, we hypothesized that miR-612 could regulate ferroptosis via the MVA pathway. Therefore, we explored the effect of miR-612 on ferroptosis. The results showed that miR-612 could promote HCC ferroptosis by increasing lipid ROS levels, thus inhibiting HCC cell proliferation and invasion. Furthermore, we explored the underlying mechanism and found that HADHA overexpression upregulated the expression of CoQ10, which is the downstream metabolite of the MVA pathway; thus, miR-612 could promote ferroptosis by downregulating CoQ10 via the HADHA-mediated MVA pathway. This finding verified our hypothesis and provided insight into the treatment of HCC by targeting the miR-612-HADHA-MVA pathway. In addition, we also found that HADHA down-expression could increase PUFA levels and lipid peroxide abundance, which could facilitate the execution of ferroptosis.

The MVA pathway is an essential metabolic pathway that uses acetyl-CoA to produce sterols and isoprenoids. We proved that HADHA upregulated the expression of MVA pathway-related enzymes (HMGCS1, HMGCR, MVD, MVK,

FPPS, GGPS1) and the regulation factor SREBP2. Lovastatin is an MVA pathway inhibitor that can inhibit HMG-CoA reductase, the key rate-limiting enzyme of the MVA pathway. Since lovastatin is commonly used in the clinic, we used lovastatin in an HCC xenograft model to evaluate the effect of miR-612 and lovastatin on ferroptosis mediated by the MVA pathway in vivo. The results showed that miR-612 and lovastatin could effectively and synergistically suppress tumor growth. Moreover, miR-612 could enhance the antitumor effect of RSL3 and lovastatin by promoting ferroptosis. Accumulating evidence has shown that statin drugs can affect tumor progression and metastasis.[33–35] Our study further proved this effect and illustrated this effect by the mechanism of ferroptosis for the first time. These results suggest that lovastatin could be a potential drug to treat cancer and that miR-612 could be an important factor facilitating this process.

Conclusions

In summary, our study revealed that miR-612 promoted HCC ferroptosis via the HADHA-mediated MVA pathway.

Data Sharing Statement

All data generated or analyzed during this study are included in this article.

Ethics Approval and Informed Consent

All experiments were approved by the Ethics Committee of Zhongshan Hospital (Approval No. B2022-229).

Acknowledgments

We sincerely thank the staff of the Liver Cancer Institute, Zhongshan Hospital, Key Laboratory of Carcinogenesis and Cancer Invasion (Ministry of Education) for their assistance with this study.

Funding

The study was supported by the National Natural Science Foundation of China (82073216), Shanghai Science and Technology Committee (20S11906300) and Shanghai Municipal Health Commission, Collaborative Innovation Cluster Project (2019CXJQ02).

Disclosure

The authors declare that they have no competing interests.

References

1. Siegel RL, Miller KD, Jemal A. Cancer statistics, 2018. *CA Cancer J Clin*. 2018;68(1):7–30. doi:10.3322/caac.21442
2. Bray F, Ferlay J, Soerjomataram I, et al. Global cancer statistics 2018: GLOBOCAN estimates of incidence and mortality worldwide for 36 cancers in 185 countries. *CA Cancer J Clin*. 2018;68(6):394–424. doi:10.3322/caac.21492
3. Al-Mehdi A, Tozawa K, Fisher A, et al. Intravascular origin of metastasis from the proliferation of endothelium-attached tumor cells: a new model for metastasis. *Nature Medicine*. 2000;6(1):100–102. doi:10.1038/71429
4. Pistritto G, Trisciuoglio D, Ceci C, et al. Apoptosis as anticancer mechanism: function and dysfunction of its modulators and targeted therapeutic strategies. *Aging*. 2016;8(4):603–619. doi:10.18632/aging.100934
5. Galluzzi L, Vitale I, Aaronson SA, et al. Molecular mechanisms of cell death: recommendations of the nomenclature committee on cell death 2018. *Cell Death Differ*. 2018;25(3):486–541. doi:10.1038/s41418-017-0012-4
6. Dixon SJ, Lemberg KM, Lamprecht MR, et al. Ferroptosis: an iron-dependent form of nonapoptotic cell death. *Cell*. 2012;149(5):1060–1072. doi:10.1016/j.cell.2012.03.042
7. Stockwell BR, Friedmann Angeli JP, Bayir H, et al. Ferroptosis: a regulated cell death nexus linking metabolism, redox biology, and disease. *Cell*. 2017;171(2):273–285. doi:10.1016/j.cell.2017.09.021
8. Kim EH, Shin D, Lee J, et al. CISD2 inhibition overcomes resistance to sulfasalazine-induced ferroptotic cell death in head and neck cancer[J]. *Cancer Lett*. 2018;432:180–190. doi:10.1016/j.canlet.2018.06.018
9. Lachaier E, Louandre C, Godin C, et al. Sorafenib induces ferroptosis in human cancer cell lines originating from different solid tumors. *Anticancer Res*. 2014;34(11):6417–6422.
10. Yang WS, SriRamaratnam R, Welsch ME, et al. Regulation of ferroptotic cancer cell death by GPX4. *Cell*. 2014;156(1–2):317–331. doi:10.1016/j.cell.2013.12.010
11. Kagan VE, Mao G, Qu F, et al. Oxidized arachidonic and adrenic PEs navigate cells to ferroptosis. *Nat Chem Biol*. 2017;13(1):81–90. doi:10.1038/nchembio.2238
12. Ang WS Y, Stockwell BR. Ferroptosis: death by lipid peroxidation. *Trends Cell Biol*. 2016;26(3):165–176. doi:10.1016/j.tcb.2015.10.014

13. Latunde-Dada GO, Latunde-Dada GO. Ferroptosis: role of lipid peroxidation, iron and ferritinophagy. *Biochim Biophys Acta Gen Subj*. 2017;1861 (8):1893–1900. doi:10.1016/j.bbagen.2017.05.019
14. Gao M, Monian P, Quadri N, et al. Glutaminolysis and transferrin regulate ferroptosis. *Mol Cell*. 2015;59(2):298–308. doi:10.1016/j.molcel.2015.06.011
15. Viswanathan VS, Ryan MJ, Dhruv HD, et al. Dependency of a therapy-resistant state of cancer cells on a lipid peroxidase pathway. *Nature*. 2017;547(7664):453–457.
16. Hangauer MJ, Viswanathan VS, Ryan MJ, et al. Drug-tolerant persister cancer cells are vulnerable to GPX4 inhibition. *Nature*. 2017;551 (7679):247–250.
17. Bartel DP. MicroRNAs: target recognition and regulatory functions. *Cell*. 2009;136(2):215–233. doi:10.1016/j.cell.2009.01.002
18. Xiao FJ, Zhang D, Wu Y, et al. miRNA-17-92 protects endothelial cells from erastin-induced ferroptosis through targeting the A20-ACSL4 axis. *Biochem Biophys Res Commun*. 2019;515(3):448–454. doi:10.1016/j.bbrc.2019.05.147
19. Zhang K, Wu L, Zhang P, et al. miR-9 regulates ferroptosis by targeting glutamic-oxaloacetic transaminase GOT1 in melanoma. *Mol, Carcinog*. 2018;57(11):1566–1576. doi:10.1002/mc.22878
20. Luo M, Wu L, Zhang K, et al. miR-137 regulates ferroptosis by targeting glutamine transporter SLC1A5 in melanoma. *Cell Death Differ*. 2018;25 (8):1457–1472. doi:10.1038/s41418-017-0053-8
21. Tao ZH, Wan JL, Zeng LY, et al. miR-612 suppresses the invasive-metastatic cascade in hepatocellular carcinoma. *J Exp Med*. 2013;210 (4):789–803. doi:10.1084/jem.20120153
22. Liu Y, Lu LL, Wen D, et al. MiR-612 regulates invadopodia of hepatocellular carcinoma by HADHA-mediated lipid reprogramming. *J Hematol Oncol*. 2020;13(1):12. doi:10.1186/s13045-019-0841-3
23. Liu W, Chakraborty B, Safi R, et al. Dysregulated cholesterol homeostasis results in resistance to ferroptosis increasing tumorigenicity and metastasis in cancer. *Nat Commun*. 2021;12(1):5103. doi:10.1038/s41467-021-25354-4
24. Li D, Wang Y, Dong C, et al. CST1 inhibits ferroptosis and promotes gastric cancer metastasis by regulating GPX4 protein stability via OTUB1. *Oncogene*. 2023;42(2):83–98. doi:10.1038/s41388-022-02537-x
25. Xi Y, Shen Y, Wu D, et al. CircBCAR3 accelerates esophageal cancer tumorigenesis and metastasis via sponging miR-27a-3p. *Mol Cancer*. 2022;21 (1):145. doi:10.1186/s12943-022-01615-8
26. Godet I, Shin YJ, Ju JA, et al. Fate-mapping post-hypoxic tumor cells reveals a ROS-resistant phenotype that promotes metastasis. *Nat Commun*. 2019;10(1):4862.
27. Hoppe U, Bergemann J, Diembeck W, et al. Coenzyme Q10, a cutaneous antioxidant and energizer. *Biofactors*. 1999;9(2–4):371–378. doi:10.1002/biof.5520090238
28. Miles MV. The uptake and distribution of coenzyme Q10. *Mitochondrion*. 2007;7(Suppl):S72–7. doi:10.1016/j.mito.2007.02.012
29. Gutierrez-Mariscal FM, Yubero-Serrano EM, Villalba JM, et al. Coenzyme Q Q(10): from bench to clinic in aging diseases, a translational review. *Crit Rev Food Sci Nutr*. 2019;59(14):2240–2257. doi:10.1080/10408398.2018.1442316
30. Bersuker K, Hendricks JM, Li Z, et al. The coq oxidoreductase FSP1 acts parallel to GPX4 to inhibit ferroptosis. *Nature*. 2019;575(7784):688–692. doi:10.1038/s41586-019-1705-2
31. Doll S, Freitas FP, Shah R, et al. FSP1 is a glutathione-independent ferroptosis suppressor. *Nature*. 2019;575(7784):7784):693–698. doi:10.1038/s41586-019-1707-0
32. Koppula P, Lei G, Zhang Y, et al. A targetable CoQ-FSP1 axis drives ferroptosis- and radiation-resistance in KEAP1 inactive lung cancers. *Nat Commun*. 2022;13(1):2206.
33. Dorsch M, Kowalczyk M, Planque M, et al. Statins affect cancer cell plasticity with distinct consequences for tumor progression and metastasis. *Cell Rep*. 2021;37(8):110056. doi:10.1016/j.celrep.2021.110056
34. Juneja M, Kobelt D, Walther W, et al. Statin and rottlerin small-molecule inhibitors restrict colon cancer progression and metastasis via MACC1. *PLoS Biol*. 2017;15(6):e2000784. doi:10.1371/journal.pbio.2000784
35. Shibata MA. Lovastatin inhibits tumor growth and lung metastasis in mouse mammary carcinoma model: a p53-independent mitochondrial-mediated apoptotic mechanism. *Carcinogenesis*. 2004;25(10):1887–1898. doi:10.1093/carcin/bgh201